Electronic Supplementary Material (ESI) for Nanoscale.

Supporting Information

Anomalous Polarization Pattern Evolution of Raman Modes in few-layer ReS_2 by Angle-resolved Polarized Raman Spectroscopy

Ruowei Wu[1], Mei Qi[2], Qiyi Zhao[3], Yuanyuan Huang[1], Yixuan Zhou[1], and Xinlong Xu[1,*]

1. Shaanxi Joint Lab of Graphene, International Collaborative Center on Photoelectric Technology and Nano Functional Materials, State Key Laboratory of Photon-Technology in Western China Energy, Institute of Photonics & Photon-Technology, Northwest University, Xi'an 710069, China.

2. School of Information Science and Technology，Northwest University，Xi'an 710127, China.

3. School of Science, Xi'an University of Posts & Telecommunications, Xi'an 710121, China.

**Corresponding author, Fax: +86-29-88303667. E-mail:*

xlxuphy@nwu.edu.cn (Xinlong Xu)

1. AFM images of ReS_2 flakes with different layers

The ReS_2 flakes were prepared by mechanical exfoliation from bulk crystal and transferred onto Si/SiO_2 substrate. The AFM images corresponding to the 2, 3, 5, 6, 11, 12, 13, and 17 layers of ReS_2 flakes in our experiment are shown in Figure S1. Due to the measurement range, the ReS_2 flake with 5 layers was not measured. According to the optical images, we can confirm that the C label in the main text (Fig. 1(b)) is 5 layers. It is known that deviation can be introduced in the measured thickness of few-layer samples using AFM at different scan direction[1]. In such case, the offset is needed to determine the correct thickness of few layers by AFM. In our work, ~0.6 nm is needed for the offset for 2-layer and 3-layer ReS_2. After the offset correction, the all areas as shown in Figure 1(b) are 0.7 nm per layer, which is consistent with the theoretical thickness and the contrast value measured by optical images.[2]

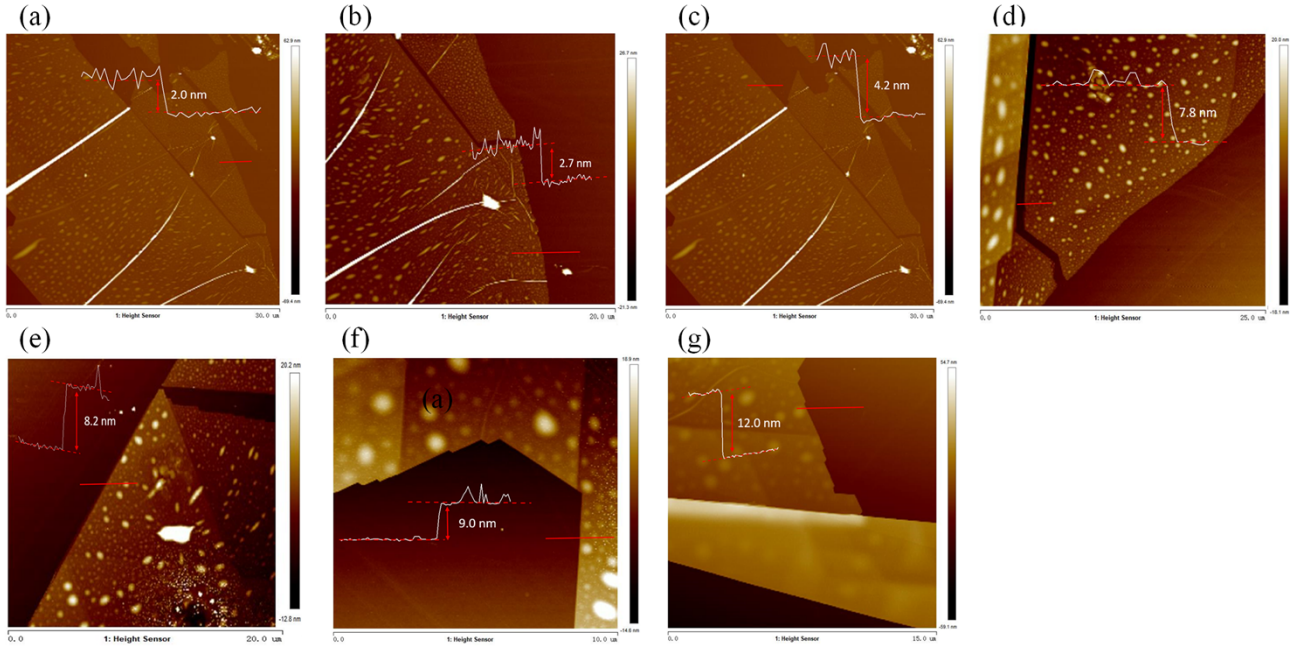

Figure S1. Atomic force microscopy (AFM) images of ReS_2 flakes. (a)-(g) correspond to the 2, 3, 6, 11, 12, 13, and 17 layers of ReS_2 flakes.

2. Schematic of angle-resolved polarized Raman spectroscopy

The sample stage is along a horizontal direction and the sample normal is along the vertical direction. The incident laser is set to vertically polarized state by a polarizer. The half-wave plate in the common optical path is used to change the polarization of excitation beam and the scattering beam. The analyzer is set to detect the vertically or horizontally polarized Raman signal. The configuration is $\theta_L V_R$ for vertically polarized Raman signal. The configuration is $\theta_L H_R$ for horizontally polarized Raman signal. The subscripts L and R correspond to laser beam and scattering beam, respectively.[3] The θ defined by the half-wave plate is the angle between the polarization of incident beam and the y-axis as shown in Figure 1 in the main text.

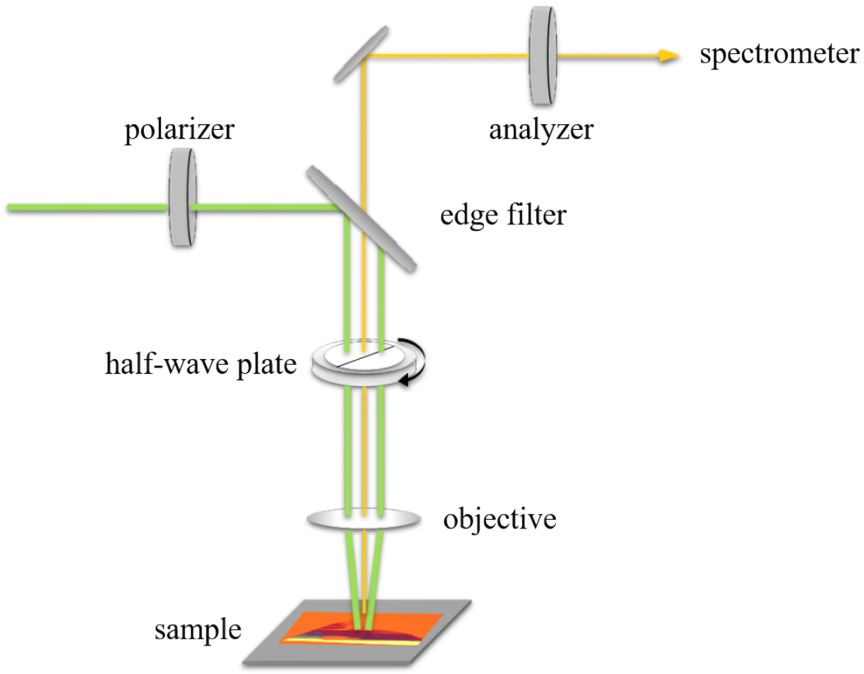

Figure S2. Schematic of angle-resolved polarized Raman spectroscopy.

3. Raman spectra of different thickness ReS_2 flakes

The Raman spectra of ReS_2 flakes with eight thicknesses (Fig.S3) contain 18 Raman modes. The intensities of mode-3 and mode-5 are larger than the other Raman modes.

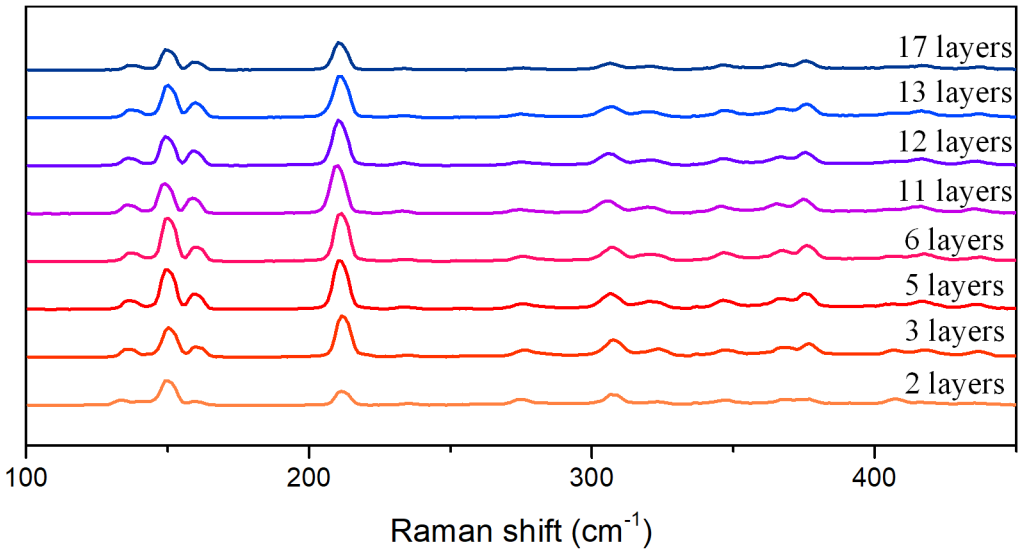

Figure S3. Raman spectra of ReS_2 with different thicknesses. The ReS_2 flakes were excited by a 532 nm linearly polarized light with a configuration of $\theta_L V_R$.

4. Raman Modes of ReS_2

MODE	2L Raman (cm^{-1})	17L Raman (cm^{-1})	Origin of phonon mode[4-5]
Mode-1	133.4	135.8	Out-of-plane vibrations of Re atoms
Mode-2	140.7	141.8	Out-of-plane vibrations of Re atoms
Mode-3	150.3	149.1	In-plane vibrations of Re atoms
Mode-4	159.9	158.7	In-plane vibrations of Re atoms
Mode-5	211.5	210.2	In-plane vibrations of Re atoms
Mode-6	235.3	232.9	In-plane vibrations of Re atoms
Mode-7	274.5	274.5	In-plane and out-of-plane vibration of Re and S atoms
Mode-8	279.5	280.4	In-plane and out-of-plane vibration of Re and S atoms
Mode-9	305.3	305.2	In-plane vibrations of S atoms
Mode-10	307.61	307.6	In-plane vibrations of S atoms
Mode-11	318.2	317.0	In-plane and out-of-plane vibrations of S atoms
Mode-12	322.9	321.7	In-plane and out-of-plane vibrations of S atoms
Mode-13	346.5	345.3	In-plane and out-of-plane vibrations of S atoms
Mode-14	367.6	366.4	In-plane and out-of-plane vibrations of S atoms
Mode-15	375.8	375.7	In-plane and out-of-plane vibrations of S atoms
Mode-16	407.3	404.9	In-plane and out-of-plane vibrations of S atoms
Mode-17	417.7	417.7	Out-of-plane vibrations of Re atoms
Mode-18	435.2	436.3	Out-of-plane vibrations of Re atoms

Table S1. The 18 Raman active modes of 17L and 2L ReS_2 under 532 nm laser excitation.

5. ARPRS of mode-3 with $\theta_L H_R$ configuration

As the in-plane vibration mode, ARPRS patterns of mode-3 demonstrate less dependent on the flake thickness with the $\theta_L H_R$ configuration. According to the formula (5) in the main text, the patterns show 4-lobes.

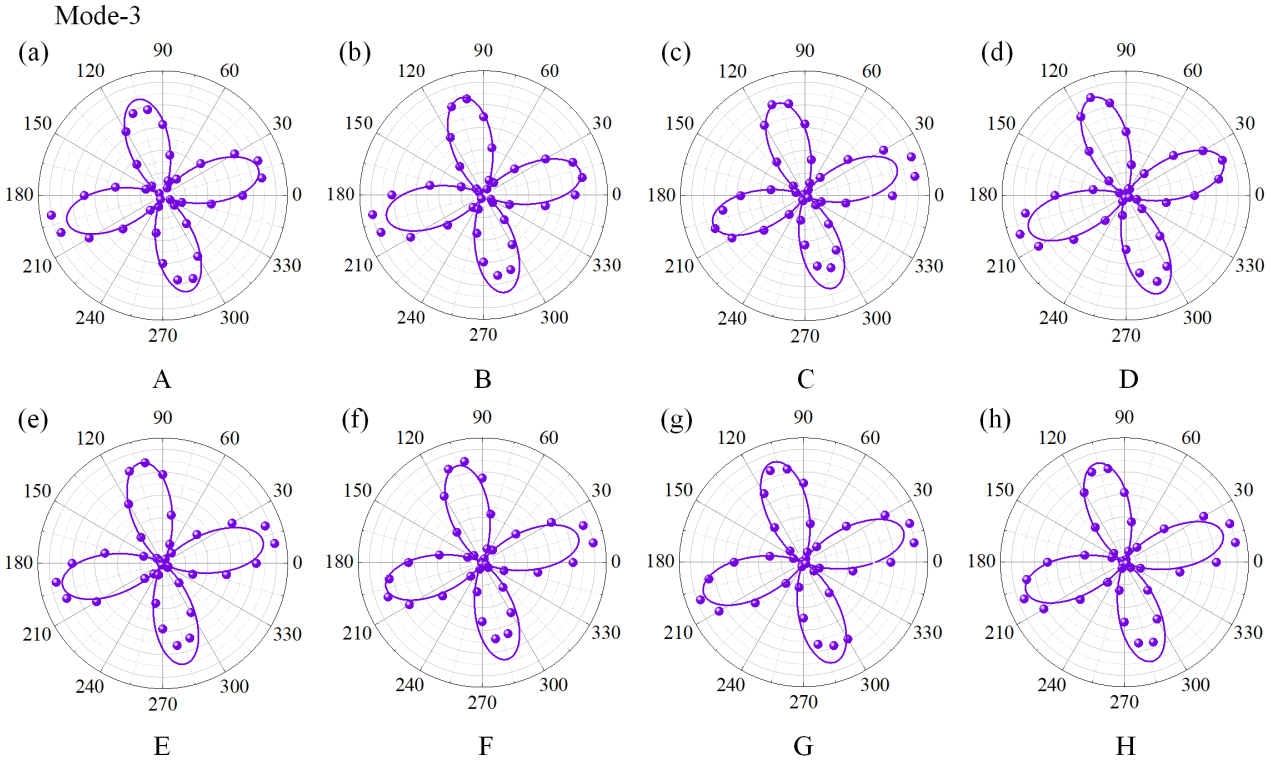

Figure S4. ARPR spectra of mode-3 with the configuration of $\theta_L H_R$. The ARPR spectra of 2, 3, 5, 6, 11, 12, 13, and 17 layers are shown in (a)~(h), respectively.

6. ARPRS of mode-5 with $\theta_L H_R$ configuration

As the in-plane vibration mode, ARPRS patterns of mode-5 are less dependent on the flake thickness with the $\theta_L H_R$ configuration. According to the formula (5), the patterns show 4-lobes.

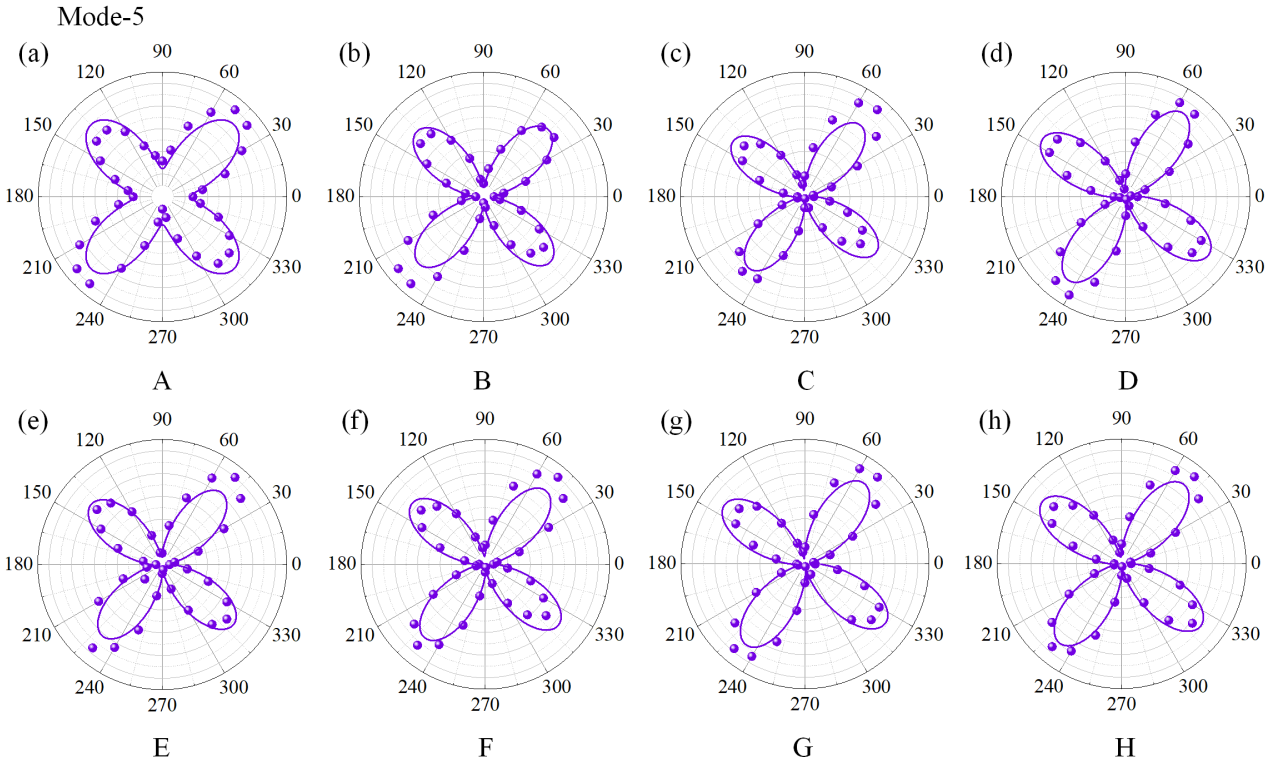

Figure S5. ARPR spectra of mode-5 with the configuration of $\theta_L H_R$. The ARPR spectra of 2, 3, 5, 6, 11, 12, 13, and 17 layers are shown in (a)~(h), respectively.

7. Color plots of the different thickness ReS_2 flakes with $\theta_L H_R$ configuration

In order to view other modes clearly, we interrupt the data at 225 cm^{-1} and demonstrate other modes in a low Raman intensity scale. The Raman intensity with the $\theta_L H_R$ configuration is much smaller than the intensity with the $\theta_L V_R$ configuration. All the patterns of 18 modes show 4-lobes with the $\theta_L H_R$ configuration.

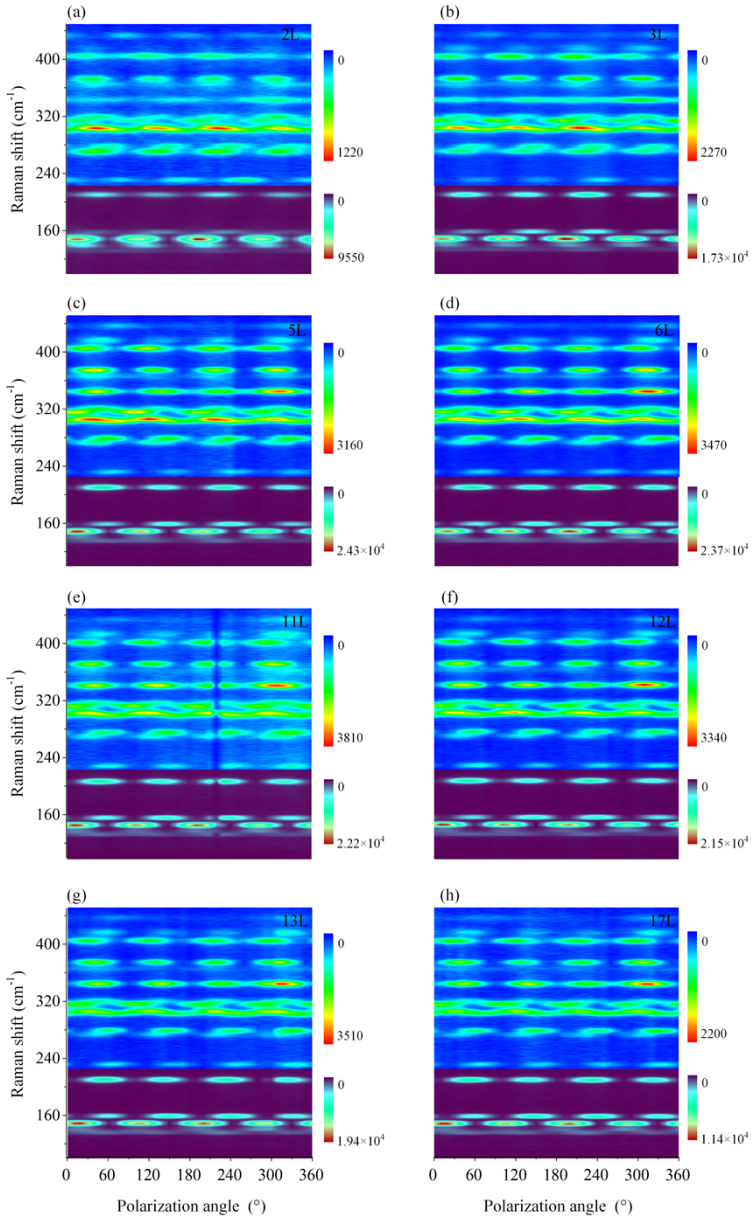

Figure S6. False color mapping of ARPRS of ReS_2 with different thicknesses under the $\theta_L H_R$ configuration. The color mapping of 2, 3, 5, 6, 11, 12, 13, and 17 layers are shown in (a)~(h), respectively..

8. ARPRS of mode-1 with $\theta_L V_R$ configuration

Mode-1 belongs to out-of-plane vibration modes. The patterns are distorted a little bit with the change of thickness.

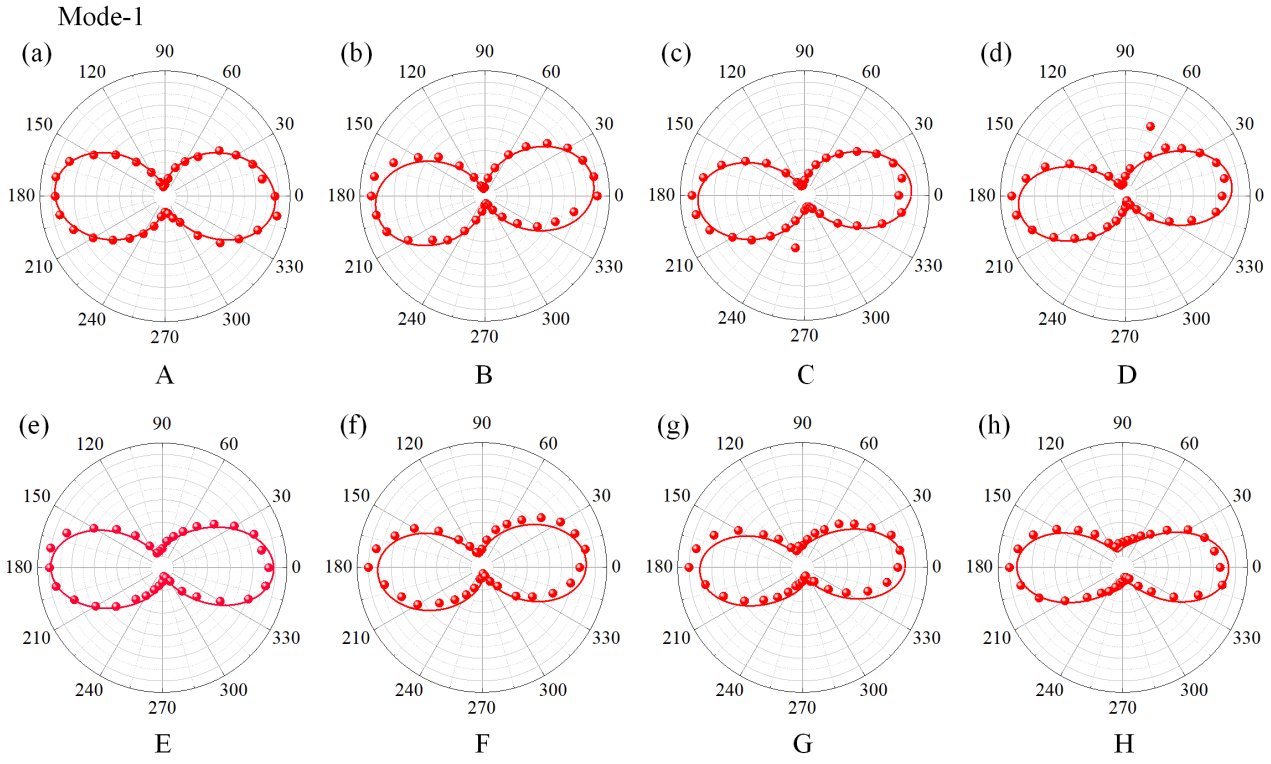

Figure S7. ARPR spectra of mode-1 with the $\theta_L V_R$ configuration. The ARPR spectra of 2, 3, 5, 6, 11, 12, 13, and 17 layers are shown in (a)~(h), respectively.

9. ARPRS of mode-2 with $\theta_L V_R$ configuration

Mode-2 belongs to out-of-plane vibration modes. The patterns of mode-2 depend on the flake thickness as shown in Fig. S8. The pattern variation is determined by the amplitude and phase of Raman elements.

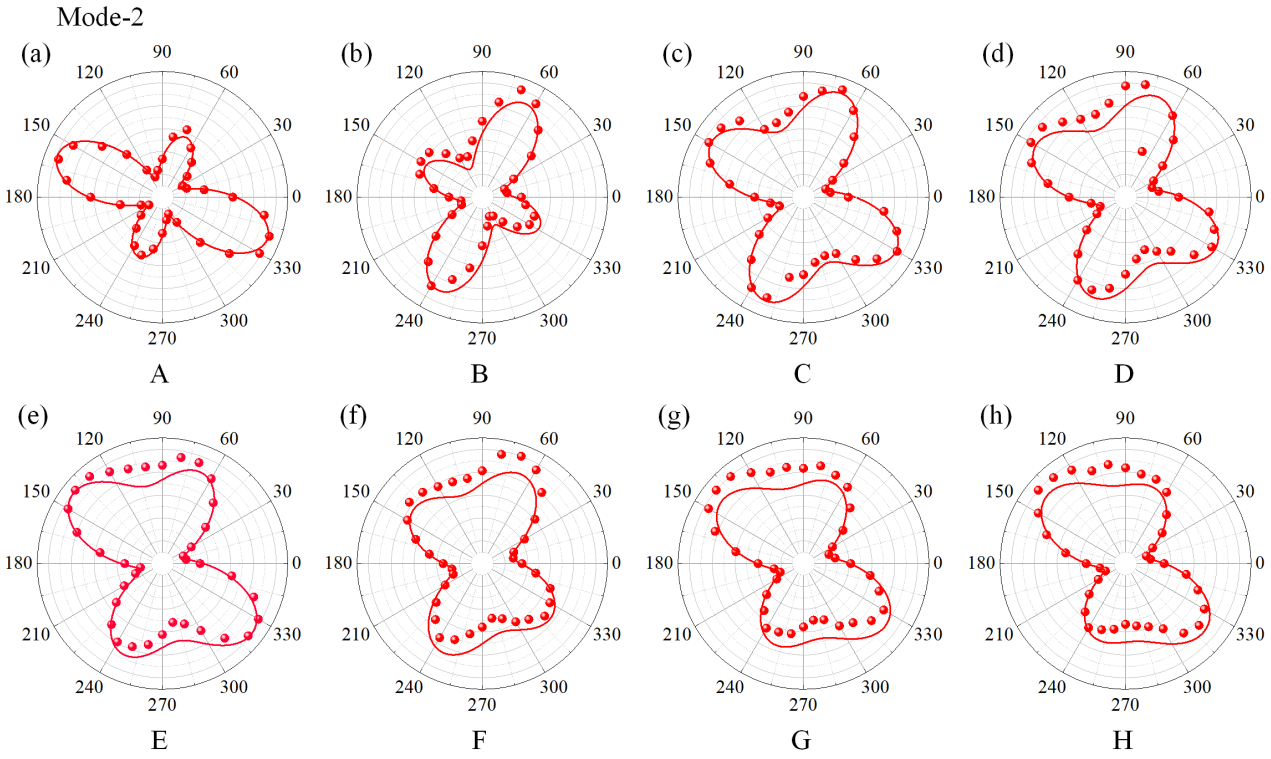

Figure S8. ARPR spectra of mode-2 with the $\theta_L V_R$ configuration. The ARPR spectra of 2, 3, 5, 6, 11, 12, 13, and 17 layers are shown in (a)~(h), respectively.

10. ARPRS of mode-3 with $\theta_L V_R$ configuration

Mode-3 belongs to in-plane vibration modes. The interlayer vibrational coupling is weak. Therefore, the patterns of mode-3 are independent on the flake thickness. This suggests that mode-3 would also be used to determine the crystalline direction, which is almost along the -30° with respect to the Re-chain direction as ReS_2 belongs to triclinic crystal system.

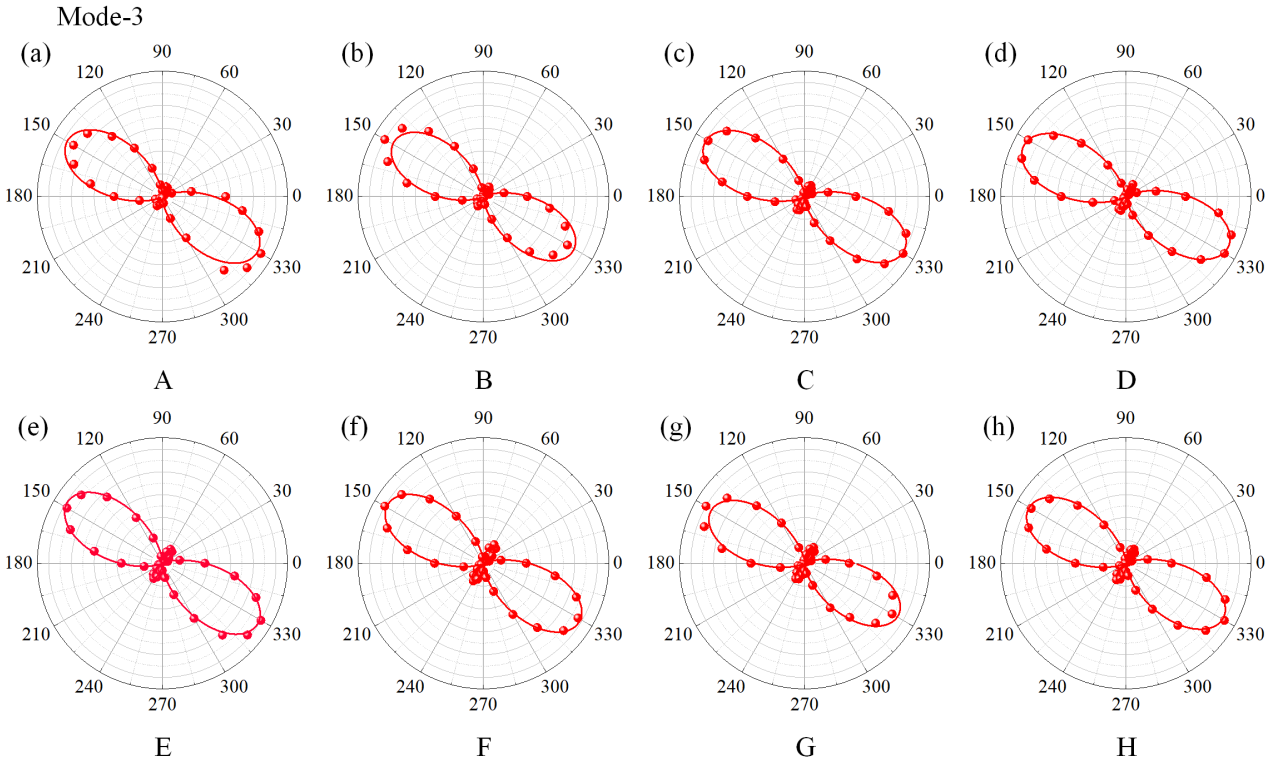

Figure S9. ARPR spectra of mode-3 with the $\theta_L V_R$ configuration. The ARPR spectra of 2, 3, 5, 6, 11, 12, 13, and 17 layers are shown in (a)~(h), respectively.

11. ARPRS of mode-4 with $\theta_L V_R$ configuration

Mode-4 belongs to in-plane vibration mode. The interlayer vibrational coupling is weak. Therefore, the patterns of mode-4 change less with the flake thickness. Especially, the maximum intensity direction keep almost the same with the flake thickness.

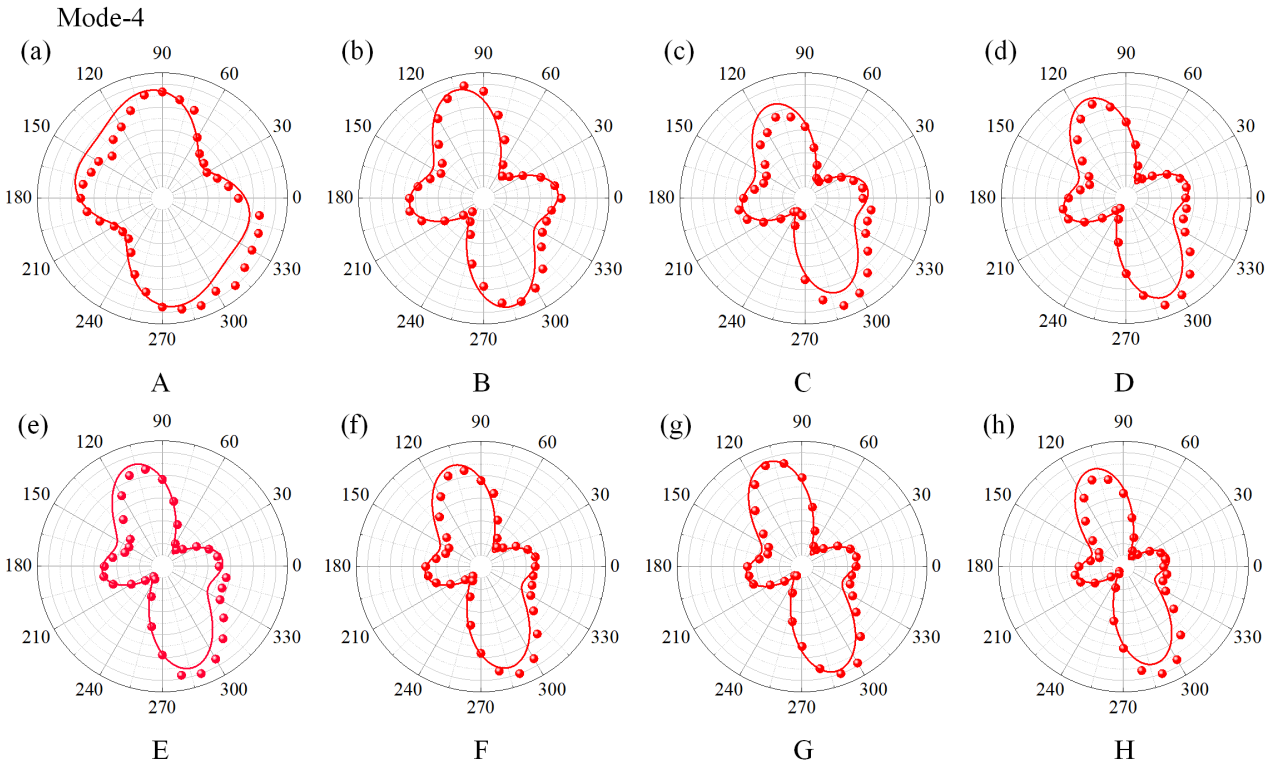

Figure S10. ARPR spectra of mode-4 with the $\theta_L V_R$ configuration. The ARPR spectra of 2, 3, 5, 6, 11, 12, 13, and 17 layers are shown in (a)~(h), respectively.

12. ARPRS of mode-5 with $\theta_L V_R$ configuration

Mode-5 belongs to in-plane vibration mode. The interlayer vibrational coupling is weak. Therefore, the patterns of mode-5 change less with thickness. The maximum intensity direction can characterize the Re-chain directions of ReS_2.

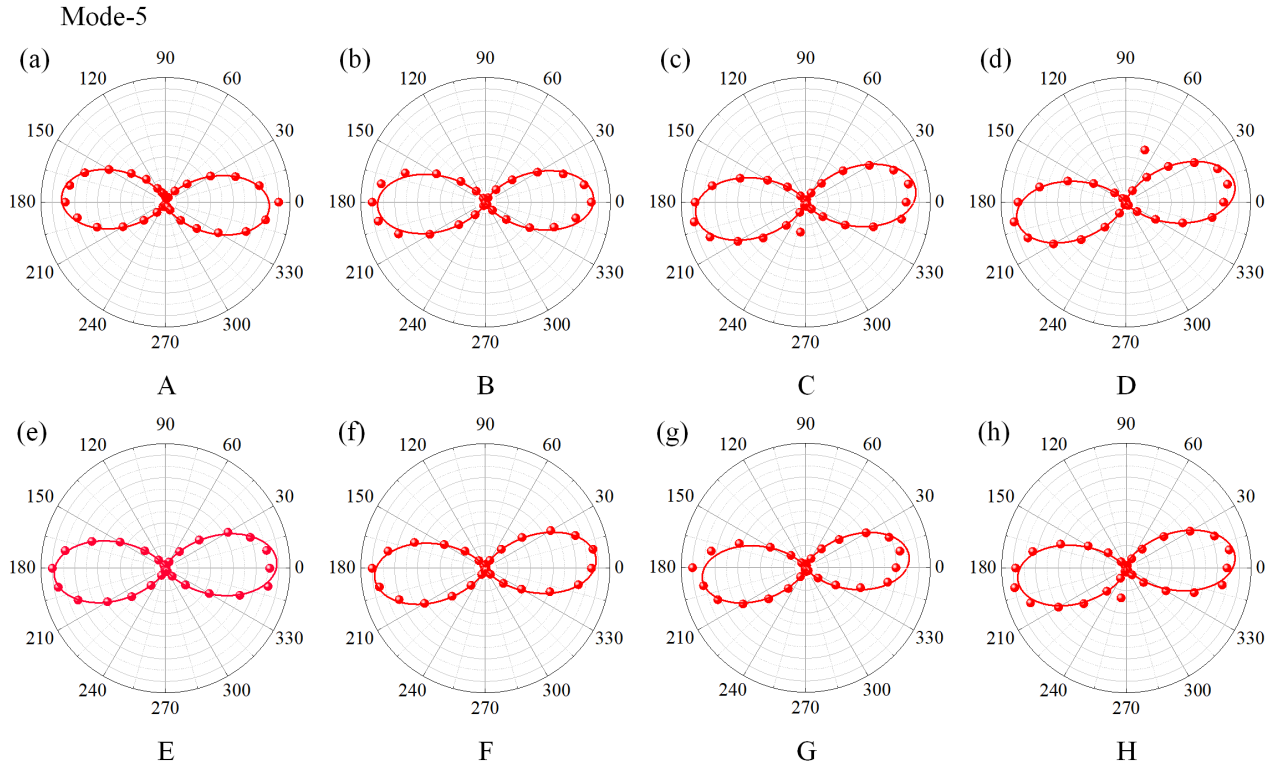

Figure S11. ARPR spectra of mode-5 with the $\theta_L V_R$ configuration. The ARPR spectra of 2, 3, 5, 6, 11, 12, 13, and 17 layers are shown in (a)~(h), respectively.

13. ARPRS of mode-8 with $\theta_L V_R$ configuration

Mode-8 is an in-plane and out-of-plane mixed mode. The interlayer vibrational coupling of mode-8 is stronger than that of in-plane vibration modes. Therefore, the patterns of mode-8 depend on the flake thickness evidently. As the few-layer ReS_2 contains strong interlayer coupling, the patterns of 2L and 3L are obviously different from those of other thicknesses.

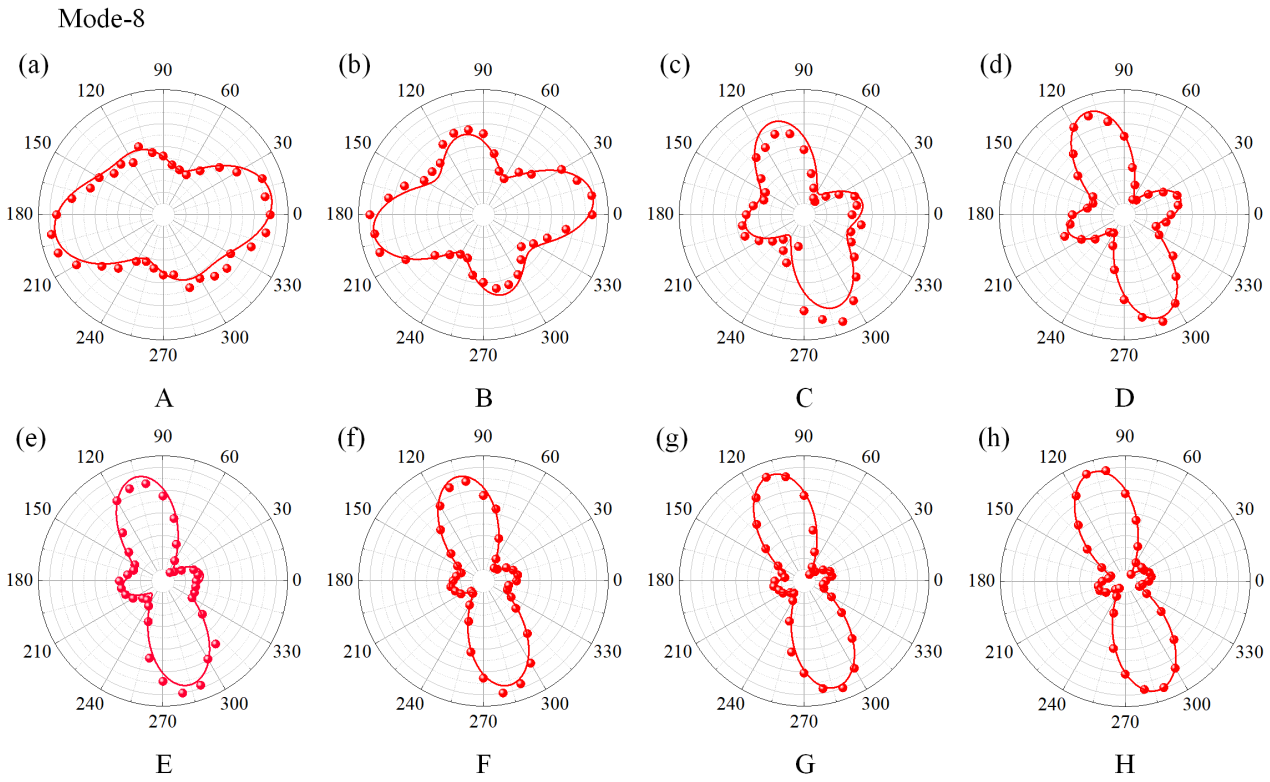

Figure S12. ARPR spectra of mode-8 with the $\theta_L V_R$ configuration. The ARPR spectra of 2, 3, 5, 6, 11, 12, 13, and 17 layers are shown in (a)~(h), respectively.

14. ARPRS of mode-15 with $\theta_L V_R$ configuration

Mode-15 is a mixed mode contains in-plane and out-of-plane vibration. The interlayer vibrational coupling of mode-15 is stronger than the in-plane vibration modes. Therefore, the patterns of mode-15 depend on the flake thickness. The pattern variations are determined by the amplitude and phase of the Raman elements.

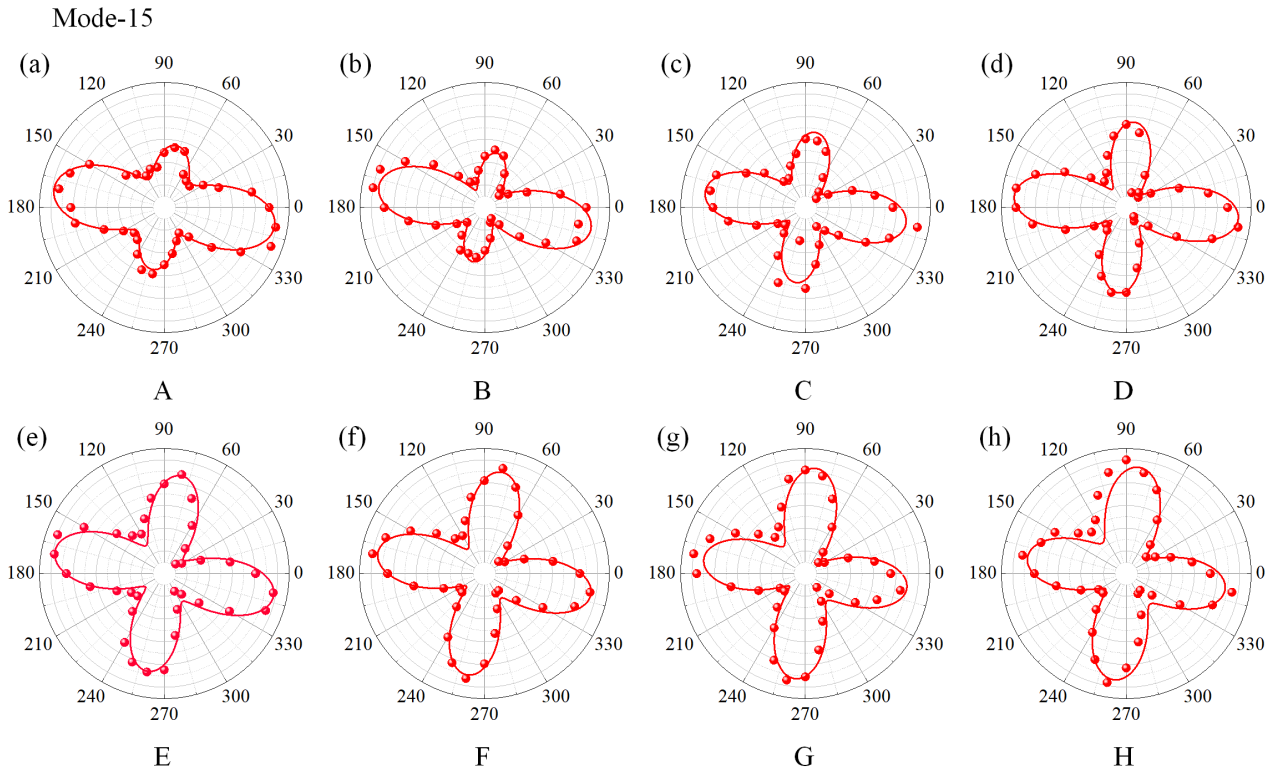

Figure S13. ARPR spectra of mode-15 with the $\theta_L V_R$ configuration. The ARPR spectra of 2, 3, 5, 6, 11, 12, 13, and 17 layers are shown in (a)~(h), respectively.

15. ARPRS of mode-17 with $\theta_L V_R$ configuration

Mode-17 belongs to the out-of-plane vibration mode. The patterns of mode-17 are influenced by the flake thickness. The pattern variation is determined by the amplitude and phase of the Raman elements.

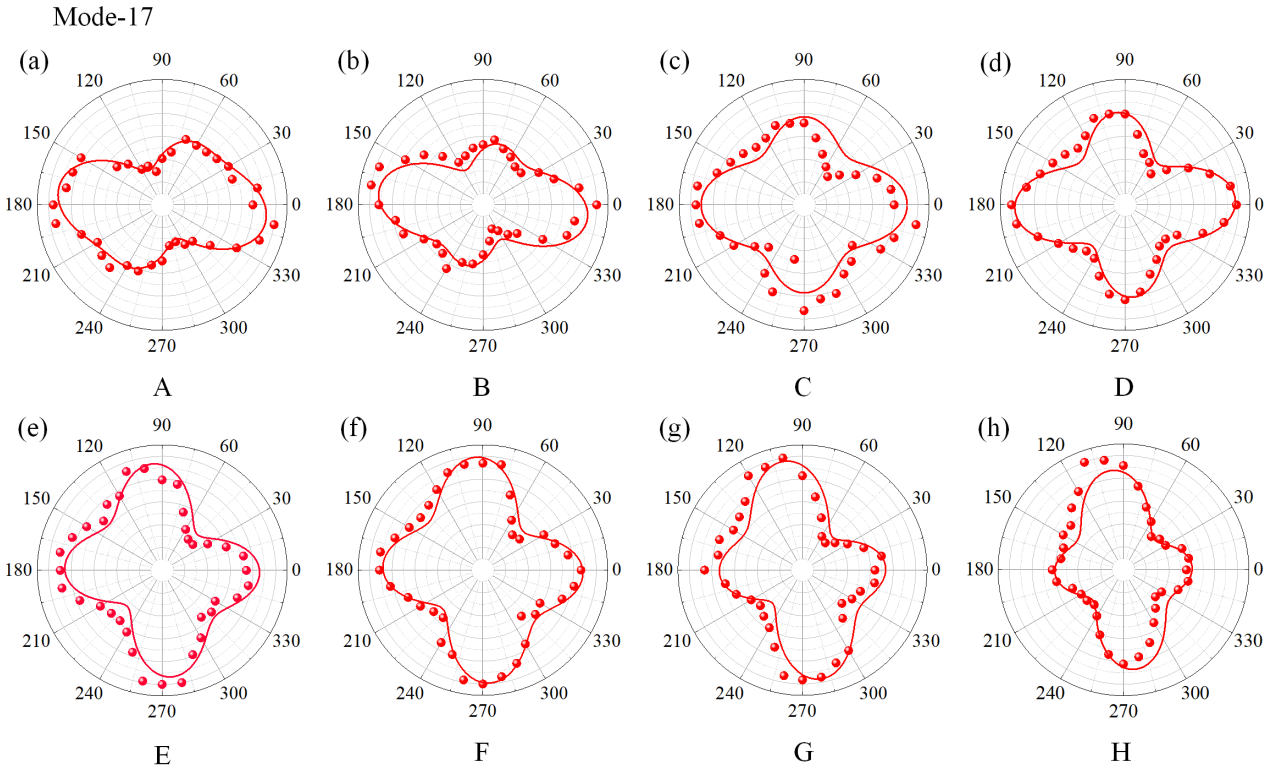

Figure S14. ARPR spectra of mode-17 with the $\theta_L V_R$ configuration. The ARPR spectra of 2, 3, 5, 6, 11, 12, 13, and 17 layers are shown in (a)~(h), respectively.

16. ARPRS of mode-18 with $\theta_L V_R$ configuration

Mode-18 belongs to the out-of-plane vibration mode. The patterns of mode-18 are distorted with the flake thickness.

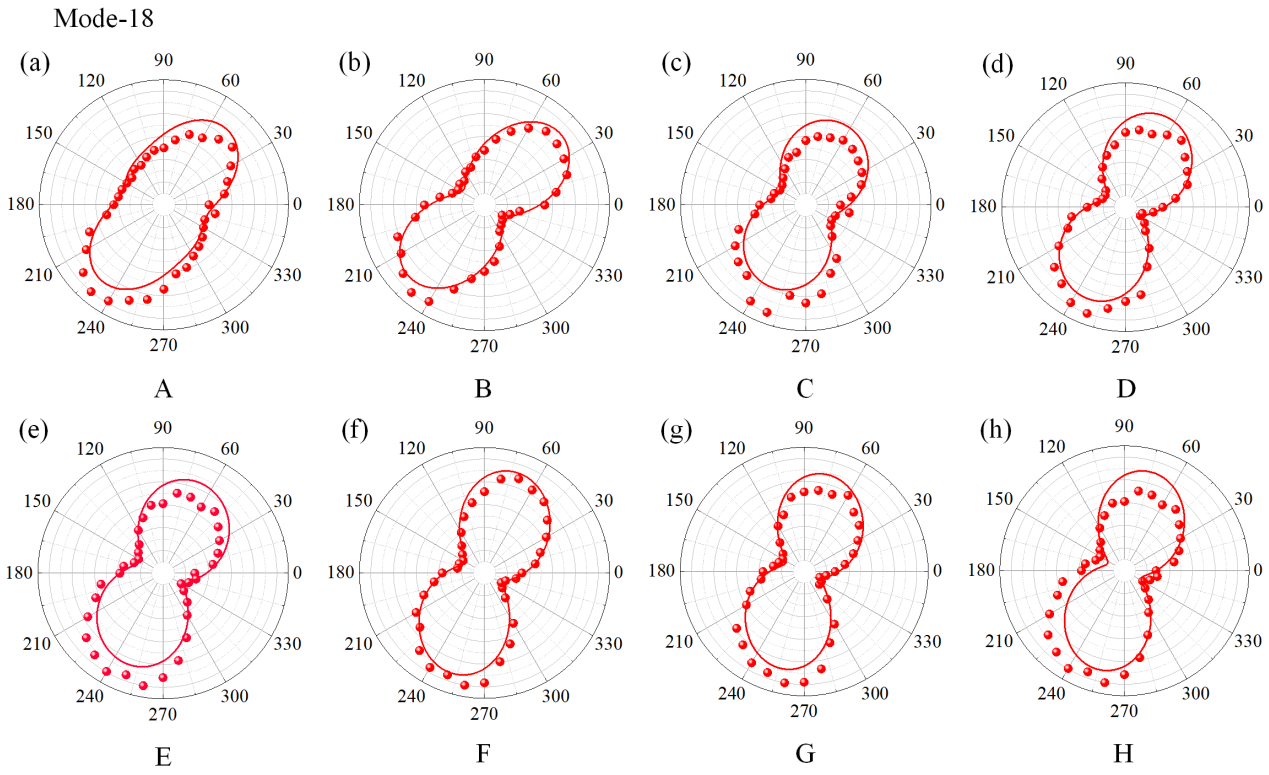

Figure S15. ARPR spectra of mode-18 with the $\theta_L V_R$ configuration. The ARPR spectra of 2, 3, 5, 6, 11, 12, 13, and 17 layers are shown in (a)~(h), respectively.

17. Coefficients of each item in formula (4)

As shown in formula (4) in the main text, the ARPRS patterns are constructed by $cos^4\theta$, $sin^4\theta$, $cos^2\theta cos^2\theta$, $cos^3\theta sin\theta$, and $cos\theta sin^3\theta$. The coefficients ($|b|^2$, $|a|^2$, $4|d|^2+2|a||b|\cos\phi_{12}$, $4|b||d|\cos\phi_{24}$, and $4|b||d|\cos\phi_{14}$) determine the contribution of different items. The amplitudes of the elements mainly determine the intensity of the items. Especially, the phase factors (ϕ_{12}, ϕ_{14}, ϕ_{24}) can lead to negative contribution of items.

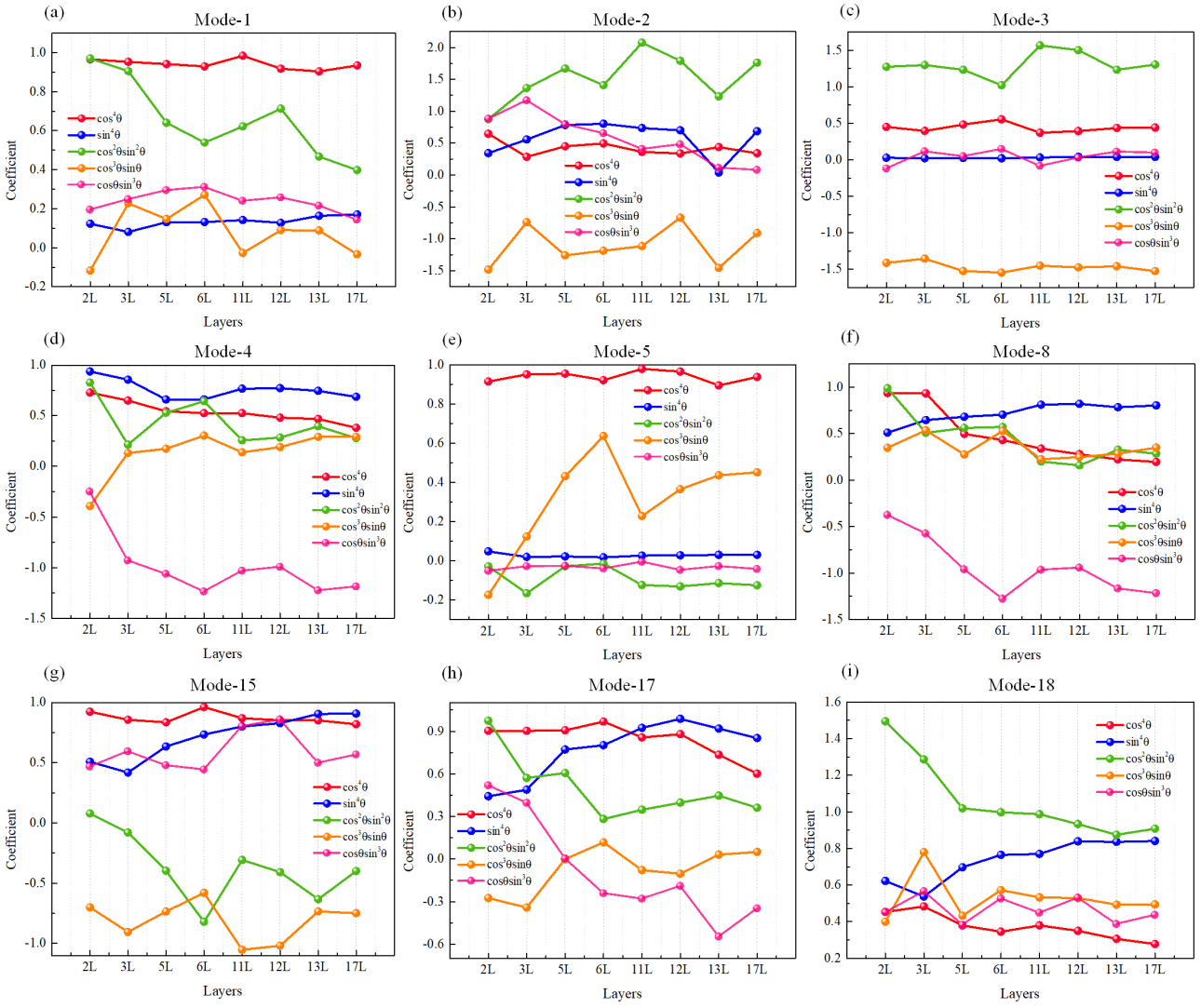

Figure S16. Coefficients of each item in formula (4) of mode-1, 2, 3, 4, 5, 15, 17, and 18 with different flake thicknesses. The coefficients of mode-1, 2, 3, 4, 5, 15, 17 and 18 are shown in (a)~(i), respectively.

18. Intensity of each item in formula (4) for 2L ReS_2

The contribution of each item in formula (4) to different modes are significantly different. The mode-1 and mode-5 are mainly determined by $cos^4\theta$. Furthermore, the petals of ARPRS patterns are determined by different items, such as mode-15. Due to the negative values, the petal along 60° to 240° for mode-3 becomes very small. For the out-of-plane vibration modes, the maximum Raman intensity is a deviated from crystalline axis and the pattern is also distorted from the standard trigonometric functions.

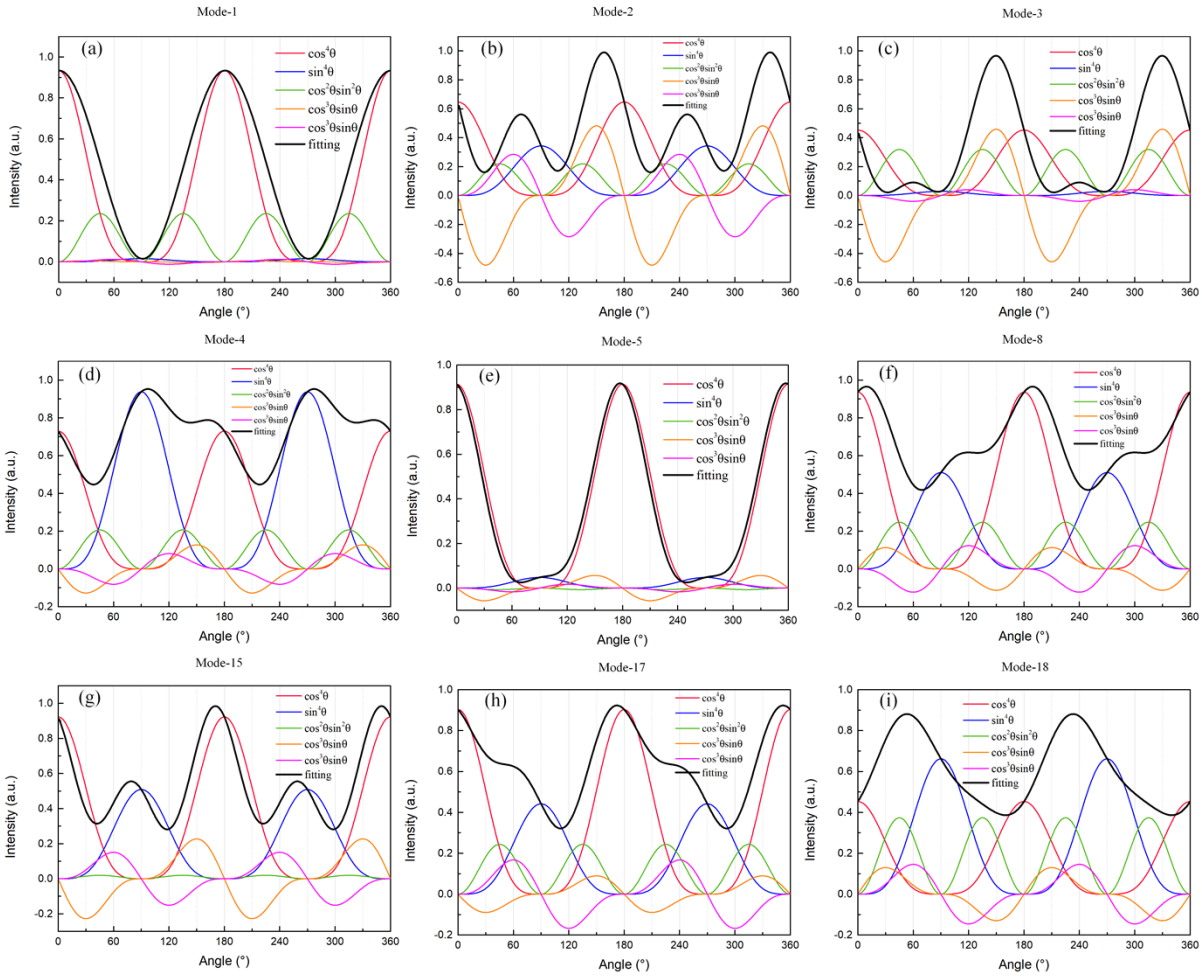

Figure S17. The intensity of each item in formula (4) for the mode-1, 2, 3, 4, 5, 15, 17, and 18 for 2L ReS_2. The intensity of each item for mode-1, 2, 3, 4, 5, 15, 17 and 18 are shown in (a)~(i), respectively.

19. Intensity of each item in formula (4) for mode-17

The maximum Raman intensity changes with the flakes thickness due to the amplitude of $cos^4\theta$ and $sin^4\theta$. The positive $cos\phi_{24}$ leads to the coupling intensity change between Raman elements and introduce pattern distortion for 2L and 3L ReS_2 flake. The amplitude of the Raman elements mainly determine the intensity of the items in formula (4). The phase factors determine the superposition relationship of each item in formula (4).

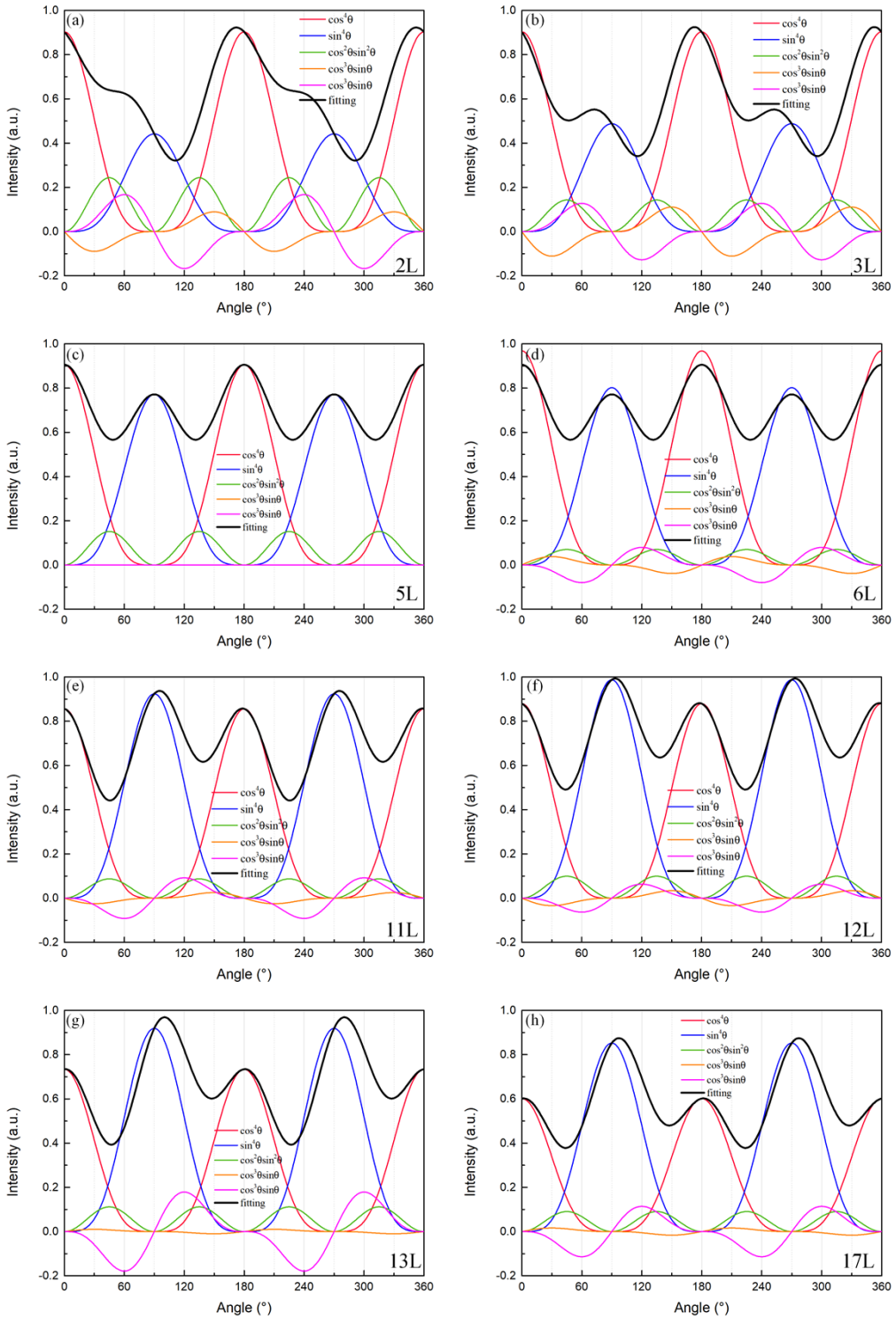

Figure S18. The intensity of each item in formula (4) of mode17 with different flake thicknesses. Intensity of each item for the 2L, 3L, 5L, 6L, 11L, 12L, 13L and 17L are shown in (a)~(i), respectively.

20. Refraction index of ReS_2 and the contribution of birefringence to pattern changes

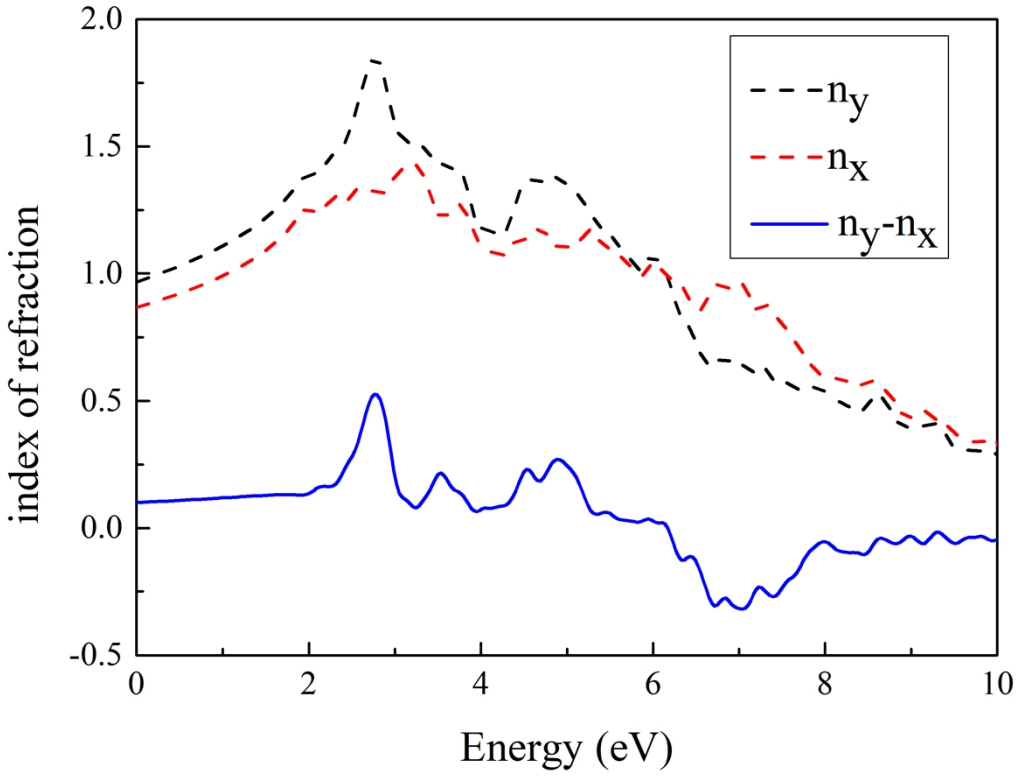

Figure S19. The refraction index of ReS_2 (monolayer) and the refraction difference (Δn). The refraction index is calculated by first principles calculation.

The phase delay (δ) due to optical birefringence causes the ARPRS pattern changes with the flake thickness[6-7]. In order to obtain the contribution of birefringence to the ARPRS pattern changes, we calculate the refraction index of ReS_2 as show in the Figure S19. According to the refraction index of monolayer ReS_2, the Δn is 0.5 when the incident laser wavelength is 532 nm. The phase shift (δ) is correlated to the sample thickness:

$$\delta = 2\pi \frac{\Delta n \cdot z}{\lambda}$$

Where Δn is the difference of refractive index, z is the thickness of the ReS_2 flake, and λ is the laser wavelength. If the thickness of ReS_2 flake is 10 nm, the value of δ approaches to 0 and the $\cos(\delta) \approx 1$. Therefore, the birefringence is not the main reason for pattern changes with the thickness in our

experiment.

Computational method: Electronic, and dielectric properties of ReS_2 have been performed through the Vienna ab initio Simulation Package (VASP)[8-9]. The Green−Wannier (GW) version of the Perdew, Burke, and Ernzerhof (PBE) parametrization has been used for the generalized gradient approximation (GGA). Projector-augmented wave (PAW) pseudopotentials act as exchange correlation and electronion interaction for all calculations.

21. Formula derivation of phase delay (δ)

If the ReS_2 flake is thick enough, the phase delay (δ) cannot be ignored. The contribution of phase delay (δ) should be considered in the fitting formula. The intensity of the polarized Raman can be described by:

$$I \propto \sum_j \left| e_R \cdot J_1 \cdot J_2 \cdot R_j \cdot J_2 \cdot J_1 \cdot e_L \right|^2 \tag{S1}$$

Jones matrix of half-wave plate (J_1) is introduced as follows:

$$J_1 = \begin{pmatrix} -\cos\theta & \sin\theta & 0 \\ \sin\theta & \cos\theta & 0 \\ 0 & 0 & 0 \end{pmatrix} \tag{S2}$$

Jones matrix of δ in the anisotropic materials (J_2) is introduced as follows:

$$J_2 = \begin{pmatrix} 1 & 0 & 0 \\ 0 & e^{i\delta} & 0 \\ 0 & 0 & 0 \end{pmatrix} \tag{S3}$$

Combining the Raman tensor:

$$R(A_g) = \begin{pmatrix} |a|e^{i\phi_1} & |d|e^{i\phi_4} & |e|e^{i\phi_5} \\ |d|e^{i\phi_4} & |b|e^{i\phi_2} & |f|e^{i\phi_6} \\ |e|e^{i\phi_5} & |f|e^{i\phi_6} & |c|e^{i\phi_3} \end{pmatrix} \tag{S4}$$

The incident laser is $\boldsymbol{e_L}$=(0 1 0), while Raman scattering signal is expressed as $\boldsymbol{e_R}$=(0 1 0) and (1 0 0) for $\theta_L V_R$ and $\theta_L H_R$ configuration, respectively.

Thus, the intensity of Raman mode can be described as：

$$\begin{aligned} I^{\theta_L V_R}(A_g) \propto & |b|^2 cos^4\theta + |a|^2 sin^4\theta + 4|d|^2 cos^2\theta sin^2\theta \\ & +4|b||d| cos^3\theta sin\theta cos\phi_{24} cos\delta \\ & +2|a||b| cos^2 sin^2\theta cos\phi_{12} cos2\delta \\ & +4|a||d| cos\theta sin^3\theta cos\phi_{14} cos\delta \end{aligned} \tag{S5}$$

REFERENCES

1. Nemes-Incze, P.; Osváth, Z.; Kamarás, K.; Biró, L. P., Anomalies in thickness measurements of graphene and few layer graphite crystals by tapping mode atomic force microscopy. *Carbon* **2008,** *46* (11), 1435-1442.

2. Wang, Y. Y.; Gao, R. X.; Ni, Z. H.; He, H.; Guo, S. P.; Yang, H. P.; Cong, C. X.; Yu, T., Thickness identification of two-dimensional materials by optical imaging. *Nanotechnology* **2012,** *23* (49), 495713.

3. Liu, X.-L.; Zhang, X.; Lin, M.-L.; Tan, P.-H., Different angle-resolved polarization configurations of Raman spectroscopy: A case on the basal and edge plane of two-dimensional materials. *Chin. Phys. B* **2017,** *26* (6), 067802.

4. Rahman, M.; Davey, K.; Qiao, S.-Z., Advent of 2D Rhenium Disulfide (ReS_2): Fundamentals to Applications. *Adv. Funct. Mater.* **2017,** *27* (10), 1606129.

5. Feng, Y.; Zhou, W.; Wang, Y.; Zhou, J.; Liu, E.; Fu, Y.; Ni, Z.; Wu, X.; Yuan, H.; Miao, F.; Wang, B.; Wan, X.; Xing, D., Raman vibrational spectra of bulk to monolayer ReS_2 with lower symmetry. *Phys. Rev. B* **2015,** *92* (5), 054110.

6. Kranert, C.; Sturm, C.; Schmidt-Grund, R.; Grundmann, M., Raman Tensor Formalism for Optically Anisotropic Crystals. *Phys. Rev. Lett.* **2016,** *116* (12), 127401-1-127401-5.

7. Zhang, S.; Mao, N.; Zhang, N.; Wu, J.; Tong, L.; Zhang, J., Anomalous Polarized Raman Scattering and Large Circular Intensity Differential in Layered Triclinic ReS_2. *ACS Nano* **2017,** *11* (10), 10366-10372.

8. Kresse, G.; Furthmüller, J., Efficient iterative schemes for ab initio total-energy calculations using a plane-wave basis set. *Phys. Rev. B* **1996,** *54* (16), 11169-11186.

9. Kresse, G.; Furthmüller, J., Efficiency of ab-initio total energy calculations for metals and semiconductors using a plane-wave basis set. *Comput. Mater. Sci.* **1996,** *6* (1), 15-50.